VOLUME 22 NUMBER 11

ACCOUNTS OF CHEMICAL RESEARCH®

NOVEMBER 1989

Chemical Bonding and Electronic Instability in Molybdenum Oxide Metals

MYUNG-HWAN WHANGBO*

Department of Chemistry, North Carolina State University, Raleigh, North Carolina 27695-8204

ENRIC CANADELL*

Laboratoire de Chimie Théorique, Université de Paris-Sud, 91405 Orsay, France

Received June 9, 1989 (Revised Manuscript Received August 14, 1989)

A number of studies have been carried out on binary and ternary molybdenum oxides because most of them are low-dimensional metals and therefore exhibit interesting physical properties associated with their electronic instabilities.[1] Red bronze $A_{0.33}MoO_3$ (A = Li, K, Rb, Cs, Tl)[2-7] is a semiconductor, while the Magnéli phases Mo_4O_{11}[8-10] and Mo_8O_{23},[11,12] blue bronze $A_{0.3}MoO_3$ (A = K, Rb, Tl),[13-15] purple bronze $A_{0.9}Mo_8O_{17}$ (A = Li, Na, K, Tl),[16-21] and rare-earth bronze $La_2Mo_2O_7$[22-24] are all metals at room temperature. Structurally, all of these oxides contain molybdenum–oxygen (Mo–O) layers made up of edge- and corner-sharing MoO_6 octahedra, with large and structurally complex unit cells. Consequently, in understanding the properties of such complex systems, it is desirable to have a few guidelines by which to single out the parts of their crystal structures and chemical bonding essential for the description of their electronic properties.

From the viewpoint of one-electron-band electronic structure, a metal is a system whose highest occupied band is partially filled, and electronic instabilities toward a metal–insulator transition [e.g., charge density

Myung-Hwan Whangbo's biography has appeared in a previous issue (*Acc. Chem. Res.* **1983**, *16*, 95). He is a Professor of Chemistry at North Carolina State University, where he has continued his research on the crystal structure–electronic property relationships in organic and inorganic low-dimensional metals. Myung-Hwan Whangbo dedicates this work to Professor Ikchoon Lee on the occasion of his 60th birthday.

Enric Canadell was born in Catalonia and was educated at the Universitat de Barcelona. He pursued his graduate work at Universidad Autonoma de Madrid, where he received his Ph.D. degree in 1976. After postdoctoral work with Lionel Salem at Universite de Paris-Sud, Orsay, France, he returned to Catalonia as an Associate Professor at the Chemistry Faculty of Tarragona. Since 1984 he has been with the CNRS working at Universite de Paris-Sud. He is currently interested in understanding the relationship between the crystal structure and physical properties of solids.

(1) For recent reviews, see: (a) Greenblatt, M. *Chem. Rev.* **1988**, *88*, 31. (b) *Low-Dimensional Properties of Molybdenum Bronzes and Oxides*; Schlenker, C., Ed.; Reidel: Dordrecht, The Netherlands, 1989.

(2) (a) Ganne, M.; Dion, M.; Boumaza, A. *C. R. Acad. Sci., Ser. 2* **1986**, *302*, 635. (b) Tsai, P. P.; Potenza, J. A.; Greenblatt, M. *J. Solid State Chem.* **1987**, *69*, 329. (c) Stephenson, N. C.; Wadsley, A. D. *Acta Crystallogr.* **1965**, *18*, 241. (d) Reau, J.-M.; Fouassier, C.; Hagenmuller, P. *Bull. Soc. Chim. Fr.* **1971**, *8*, 2884.

(3) (a) Bang, G.; Sperlich, G. *Z. Phys. B* **1975**, *22*, 1. (b) Travaglini, G.; Wachter, P.; Marcus, J.; Schlenker, C. *Solid State Commun.* **1982**, *42*, 407.

(4) Whangbo, M.-H.; Evain, M.; Canadell, E.; Ganne, M. *Inorg. Chem.* **1989**, *28*, 267.

(5) Tsai, P. P.; Potenza, J.; Greenblatt, M.; Schugar, H. J. *J. Solid State Chem.* **1986**, *64*, 47.

(6) (a) Collins, B. T.; Ramanujachary, K. V.; Greenblatt, M.; McCarroll, W. H.; McNally, P.; Waszczak, J. V. *J. Solid State Chem.* **1988**, *76*, 319. (b) Strobel, P.; Greenblatt, M. *J. Solid State Chem.* **1981**, *36*, 331.

(7) Canadell, E.; Whangbo, M.-H. *Inorg. Chem.* **1988**, *27*, 228.

(8) (a) Ghedira, M.; Vincent, H.; Marezio, M.; Marcus, J.; Fourcadot, G. *J. Solid State Chem.* **1985**, *56*, 66. (b) Kihlborg, L. *Ar. Kemi* **1963**, *21*, 365. (c) Magnéli, A. *Acta Chem. Scand.* **1948**, *2*, 861.

(9) (a) Schlenker, C.; Dumas, J. *Crystal Structures and Properties of Materials with Quasi-One-Dimensional Structures*; Rouxel, J., Ed.; Reidel: Dordrecht, The Netherlands, 1986; p 135. (b) Guyot, H.; Schlenker, C.; Pouget, J. P.; Ayroles, R.; Roucau, C. *J. Phys. C* **1985**, *18*, 427. (c) Guyot, H.; Schlenker, C.; Fourcadot, G.; Konate, K. *Solid State Commun.* **1985**, *54*, 909. (d) Guyot, H.; Escribe-Filippini, C.; Fourcadot, G.; Konate, K.; Schlenker, C. *J. Phys. C* **1983**, *16*, L1227.

(10) Canadell, E.; Whangbo, M.-H.; Schlenker, C.; Escribe-Filippini, C. *Inorg. Chem.* **1989**, *28*, 1466.

(11) (a) Fujishita, H.; Sato, M.; Sato, S.; Hoshino, S. *J. Solid State Chem.* **1987**, *66*, 40. (b) Magnéli, A. *Acta Chem. Scand.* **1948**, *2*, 501.

(12) (a) Sato, M.; Nakao, K.; Hoshino, S. *J. Phys. C* **1984**, *17*, L817. (b) Sato, M.; Fujishita, H.; Sato, S.; Hoshino, S. *J. Phys. C* **1986**, *19*, 3059.

(13) (a) Ghedira, M.; Chenavas, J.; Marezio, M.; Marcus, J. *J. Solid State Chem.* **1985**, *57*, 300. (b) Ganne, M.; Boumaza, A.; Dion, M.; Dumas, J. *Mater. Res. Bull.* **1985**, *20*, 1297. (c) Graham, J.; Wadsley, A. D. *Acta Crystallogr.* **1966**, *20*, 93.

0001-4842/89/0122-0375$01.50/0

wave (CDW) or spin density wave (SDW) formation] occur when the Fermi surface of the partially filled band is nested.[10,15,18,21,24] In all the molybdenum oxides except for rare-earth bronze $La_2Mo_2O_7$, the average d-electron count on Mo is less than d^1. Thus, in a molybdenum oxide metal containing several nonequivalent Mo atoms per unit cell, only a limited number of Mo atoms may have d electrons and hence be responsible for its metallic character. Consequently, in discussing the structural and electronic properties of molybdenum oxide metals, it is important to analyze how the Mo atoms possessing d electrons can be identified on the basis of their crystal structures, which d orbitals of such Mo atoms contribute to form the highest occupied bands, what kinds of dispersion relations and Fermi surfaces these bands have, and finally, how the Fermi surfaces are related to their electronic instabilities. In the present Account, we discuss both conceptual and practical aspects of those questions and show that the electronic properties of low-dimensional metals possessing large and complex unit cells can be readily understood by analyzing how the nature of their highest occupied bands is related to the crystal structures.

Distortion and Lowest Lying d-Block Level

MoO_6 octahedra of molybdenum oxides are distorted in shape, so their t_{2g}-block levels are split in energy. Because of low d-electron count on Mo (less than d^1), the highest occupied band of a molybdenum oxide is derived from the lowest lying t_{2g}-block levels of distorted MoO_6 octahedra. The t_{2g}-block levels of a regular MoO_6 octahedron have antibonding combinations between molybdenum 4d and oxygen 2p orbitals. Therefore, an Mo–O bond shortening raises any t_{2g}-block level if this level has an antibonding combination of Mo and O orbitals along the shortened Mo–O bond. Consequently, a distortion in which one Mo–O bond is shortened (see **1**) leaves one t_{2g} level (i.e., the δ orbital with respect to the shortened Mo–O bond axis) unaffected, but raises the remaining two levels (i.e., the π orbitals with respect to the shortened Mo–O bond axis).[4] On the other hand, all three t_{2g}-block levels are raised by a distortion in which two or more Mo–O bonds are shortened (see **2**).[4] Thus, inspection of the nature and extent of distortion in MoO_6 octahedra allows us to predict which MoO_6 octahedra of a given molybdenum oxide would have d electrons and what kinds of occupied d-block bands the oxide is likely to have. Alternatively, Zachariasen analysis[25] can be used to find out metal atoms of lower oxidation state, which are likely to have d electrons. However, the nature of the highest occupied d-block bands resulting from these atoms cannot be predicted by this analysis.

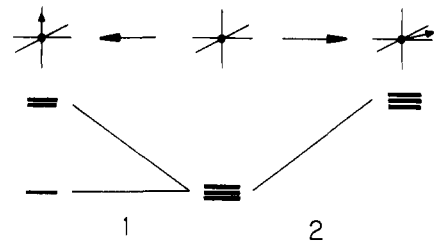

Step-Layers of MoO_6 Octahedra in Red and Blue Bronzes

Although red bronze $A_{0.33}MoO_3$ (A = K, Rb, Cs, Tl)[2,3] and blue bronze $A_{0.3}MoO_3$ (A = Na, K, Rb, Tl)[13,14] have similar chemical formulas, their crystal structures are markedly different.[2,13] Provided that side- and top-projection views of an MoO_5 single chain **3** are given by **4a** and **4b**, respectively, then **5a** and **5b** represent side- and top-projection views of an Mo_2O_9 double chain.

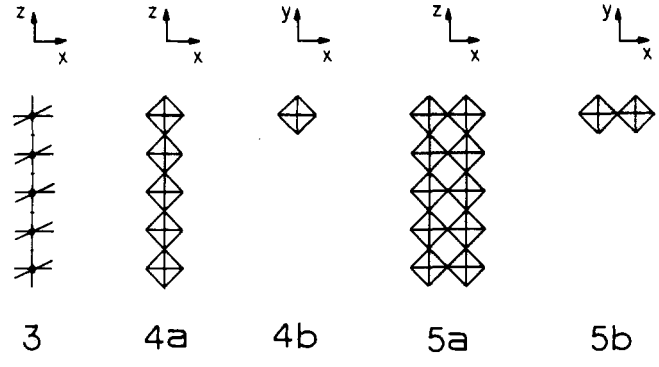

The latter is converted to an Mo_6O_{24} double chain **6** upon adding "hump" MoO_6 octahedra (shaded ones).[4,15] An Mo_6O_{18} step-layer **7** is obtained from Mo_6O_{24} chains by sharing edges and faces. Red bronze $A_{0.33}MoO_3$ (A = K, Br, Cs, Tl) has Mo_6O_{18} step-layers alternate with layers of the cations A^+.[2,4] [Lithium red bronze $Li_{0.33}MoO_3$[5] has a structure quite different from that of other red bronzes $A_{0.33}MoO_3$ (A = K, Rb, Cs, Tl) just described.] In describing the Mo–O step-layers of MoO_6 octahedra present in blue bronze $A_{0.3}MoO_3$, it is convenient to employ Mo_4O_{17} quadruple chains **8**, which lead to an Mo_4O_{13} step-layer **9** upon sharing edges.[15] An $Mo_{10}O_{30}$ step-layer **10** is obtained from **9** by adding hump MoO_6 octahedra in a half-staggered and half-eclipsed manner.[15] In **10** the "half-hidden" hump octahedra differ in their z-axis height from the other

(14) (a) Pouget, J. P.; Kagoshima, S.; Schlenker, C.; Marcus, J. *J. Phys. Lett.* **1983**, *44*, L133. (b) Fleming, R.; Schneemeyer, L. F.; Moncton, D. E. *Phys. Rev. B* **1985**, *31*, 899. (c) Tamegai, T.; Tsutsumi, K.; Kagoshima, S.; Kanai, Y.; Taui, M.; Tomozawa, H.; Sato, M.; Tsuji, K.; Harada, J.; Sakata, M.; Nakajima, T. *Solid State Commun.* **1984**, *51*, 585. (d) Pouget, J. P.; Noguera, C.; Moudden, A. H.; Moret, T. *J. Phys. (Les Ulis, Fr.)* **1985**, *46*, 1731.
(15) Whangbo, M.-H.; Schneemeyer, L. F. *Inorg. Chem.* **1986**, *25*, 2424.
(16) (a) Vincent, H.; Ghedira, M.; Marcus, J.; Mercier, J.; Schlenker, C. *J. Solid State Chem.* **1983**, *47*, 113. (b) Greenblatt, M.; Ramanujachary, K. V.; McCarroll, W. H.; Neifeld, R.; Waszczak, J. V. *J. Solid State Chem.* **1985**, *59*, 149. (c) Ganne, M.; Dion, M.; Boumaza, A.; Tournoux, M. *Solid State Commun.* **1986**, *59*, 137.
(17) (a) Ramanujachary, K. V.; Collins, B. T.; Greenblatt, M. *Solid State Commun.* **1986**, *59*, 647. (b) Escribe-Filippini, C.; Konate, K.; Marcus, J.; Schlenker, C.; Almairac, R.; Ayroles, R.; Roucau, C. *Philos. Mag. B* **1984**, *50*, 321.
(18) Whangbo, M.-H.; Canadell, E.; Schlenker, C. *J. Am. Chem. Soc.* **1987**, *109*, 6308.
(19) Onoda, M.; Toriumi, K.; Matsuda, Y.; Sato, M. *J. Solid State Chem.* **1987**, *66*, 163.
(20) (a) Greenblatt, M.; McCarroll, W. H.; Neifeld, R.; Croft, M.; Waszczak, J. V. *Solid State Commun.* **1984**, *51*, 671. (b) Schlenker, C.; Schwen, K. H.; Escribe-Filippini, C.; Marcus, J. *Physica* **1985**, *135B*, 511. (c) Matsuda, Y.; Onoda, M.; Sato, M. *Physica* **1986**, *143B*, 243.
(21) Whangbo, M.-H.; Canadell, E. *J. Am. Chem. Soc.* **1988**, *110*, 358.
(22) Moioni, A.; Subramanian, M.; Clearfield, A.; DiSalvo, F. J.; McCarroll, W. H. *J. Solid State Chem.* **1987**, *66*, 136.
(23) Collins, B. T.; Greenblatt, M.; McCarroll, W. H.; Hull, G. W. *J. Solid State Chem.* **1988**, *73*, 507.
(24) Whangbo, M.-H.; Canadell, E. *Inorg. Chem.* **1987**, *26*, 842.
(25) Zachariasen, W. H. *J. Less-Common Met.* **1978**, *62*, 1.

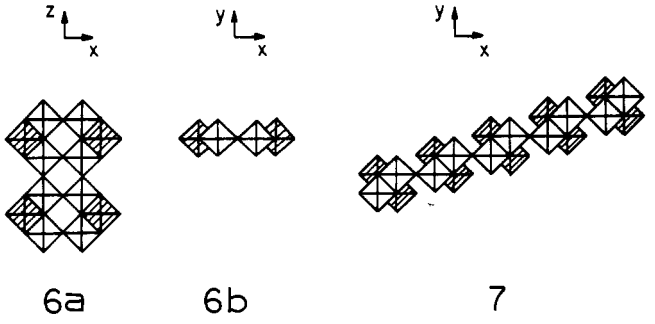

6a 6b 7

hump octahedra by half the repeat distance along the z axis. Therefore either the former or the latter octahedra have an eclipsed arrangement along the z-axis

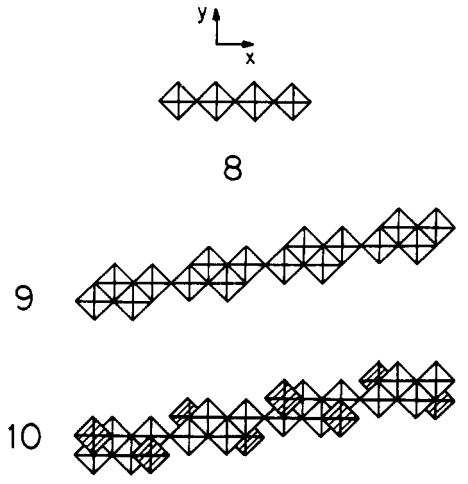

direction as in **6**, but the former are staggered to the latter in their arrangement along the z direction. It is these $Mo_{10}O_{30}$ step-layers that alternate with layers of the cations A^+ in blue bronze $A_{0.3}MoO_3$.[13,15] With the formal oxidation states of A^+ and O^{2-}, therefore, red bronze has two electrons per formula unit $A_2Mo_6O_{18}$ to fill its d-block bands, while blue bronze has three electrons per formula unit $A_3Mo_{10}O_{30}$ to fill its d-block bands. On the Mo–O step-layers of red and blue bronzes, the hump MoO_6 octahedra have a type **2** distortion, while all other MoO_6 octahedra have a type 1 distortion in which the shortened Mo–O bonds are pointed along the direction perpendicular to the step plane (i.e., along the y axis). Therefore, the bottom portions of the t_{2g}-block bands in red and blue bronzes, and hence their highest occupied bands, are mainly constructed from the xz orbitals of nonhump MoO_6 octahedra (see **11**).[4,15]

Band Dispersion and Wave Vectors

The electronic structure of a metal and hence possible electronic instabilities are typically discussed in terms of wave vectors. In describing orbital interactions among various sites of a solid, wave vectors are used in the form of mixing coefficients for site orbitals.[26] For example, the band orbital of a two-dimensional (2D) lattice with repeat distances d_1 and d_2 is expressed as

$$\phi(k_1,k_2) \propto \sum_m \sum_n \exp(ik_1md_1)\exp(ik_2nd_2)\chi_{mn}$$

where χ_{mn} is the orbital at the lattice site (m, n). All the energy levels $e(k_1,k_2)$ that the orbital $\phi(k_1,k_2)$ can have are given by the wave vectors (k_1, k_2) of the first Brillouin zone (FBZ) (e.g., $-\pi/d_1 \le k_1 \le \pi/d_1$, and $-\pi/d_2 \le k_2 \le \pi/d_2$ for a 2D rectangular lattice). To evaluate how strongly the site orbitals interact along different directions of the crystal lattice, $e(k_1,k_2)$ vs (k_1, k_2) plots are calculated along different directions of (k_1, k_2) values in the FBZ, e.g., along $\Gamma \rightarrow X$ and $\Gamma \rightarrow Y$, where Γ, X, and Y refer to the wave vector points $(k_1, k_2) = (0, 0)$, $(\pi/d_1, 0)$, and $(0, \pi/d_2)$, respectively.

The coefficients $\exp(ik_1md_1)\exp(ik_2nd_2)$ of the site orbitals χ_{mn} are particularly simple at special points such as Γ, X, and Y, where they are $(1)^m(1)^n$, $(-1)^m(1)^n$, and $(1)^m(-1)^n$, respectively. Thus at Γ, site orbitals are arranged without sign change along the d_1 and d_2 directions. At X, they are arranged with alternating signs along the d_1 direction but without sign change along the d_2 direction. For molybdenum oxides, d orbitals on any Mo–O–Mo bridge along the d_1 or d_2 direction have either the same sign (e.g., **12a**) or opposite signs (e.g., **12b**) at special wave vector points such as Γ, X, and Y. The

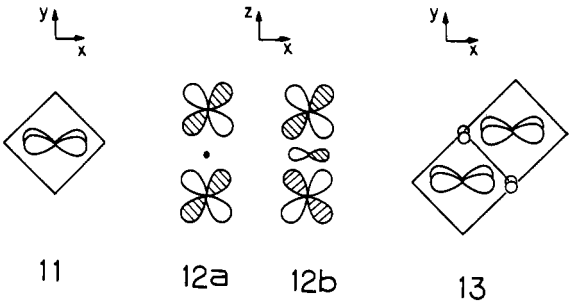

11 12a 12b 13

bridging-oxygen atom has no orbital to mix with the xz orbitals of **12a**, but has one 2p orbital to mix with those of **12b**. Since the bridging-oxygen p orbitals combines in an antibonding manner with the neighboring d orbitals in forming d-block levels (e.g., **12b**), **12b** is higher in energy than **12a**. Consequently, given an arrangement of d orbitals with the phases dictated by the point Γ, X, or Y, it is simple to determine whether or not bridging-oxygen p orbitals can mix in various Mo–O–Mo bridges. The resulting d-block band level is higher in energy when more Mo–O–Mo bridges have nonvanishing oxygen p-orbital contribution, so that qualitative features of d-block band dispersions can be explained by simply counting the number of bridging p-orbital contributions (see later for further discussions).[4,10,18,21]

Parts a and b of Figure 1 show the dispersion relations of the t_{2g}-block bands (the bottom portions) calculated for red[4] and blue[15] bronzes, respectively. Blue bronze shows a strong dispersion along the chain direction since the energy difference between **12a** and **12b** in each linear Mo–O–Mo unit is significant but a weak dispersion along the interchain direction since the xz orbitals of adjacent chains have a weak through-space interaction and a vanishing through-bond interaction due to the right-angle arrangement of Mo–O–Mo units between adjacent chains (see **13**).[4] Both red and blue bronzes have similar dispersions along the interchain direction. Along the chain direction, the bottom band of red bronze has a significantly weaker dispersion

(26) (a) Whangbo, M.-H. In *Crystal Structures and Properties of Materials with Quasi One-Dimensional Structures*; Rouxel, J., Ed.; Reidel: Dordrecht, The Netherlands, 1986; p 27. (b) Whangbo, M.-H. In *Extended Linear Chain Compounds*; Miller, J. S., Ed.; Plenum: New York, 1982; p 127.

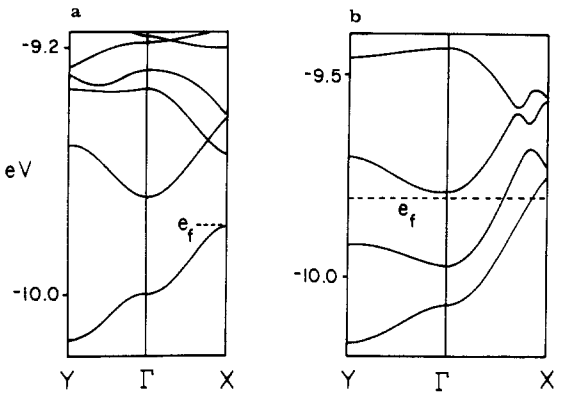

Figure 1. Dispersion relations calculated for the bottom portion of the t_{2g}-block bands in (a) red bronze and (b) blue bronze along the chain direction $\Gamma \rightarrow X$ and along the interchain direction $\Gamma \rightarrow Y$. The dashed lines refer to the Fermi levels.

compared with that of blue bronze and is therefore separated from the other bands lying above. This is due to the fact that red bronze has a stronger Mo–O–Mo···O···Mo alternation (in other words, stronger "dimerization") along the chain than does blue bronze, which essentially originates from the difference in their hump-octahedra arrangements (i.e., all eclipsed in red bronze, but half-staggered and half-eclipsed in blue bronze). Although the hump octahedra do not contribute their d orbitals to the lowest lying d-block bands, the nature of the latter is influenced by the chain distortions the hump octahedra induce. In a similar manner, the electronic structure of $Cs_{0.25}MoO_3$[27] (which is predicted to be a metal[28]) differs from that of red bronze $Cs_{0.33}MoO_3$, since their Mo–O step-layers are different in the arrangement of hump octahedra.[28]

With three electrons per formula unit $A_3Mo_{10}O_{30}$, blue bronze has the bottom two t_{2g}-block bands partially filled (Figure 1b). The dispersions of these two bands are cut by the Fermi level only in one direction (i.e., along the chain direction), so that blue bronze is a one-dimensional (1D) metal.[15] With two electrons per formula unit $A_2Mo_6O_{18}$, red bronze has the bottom t_{2g}-block band completely filled (Figure 1a), so that red bronze is a regular semiconductor (i.e., one that has no partially filled band in a one-electron picture).[4] It has been suggested[29] that red bronze $K_{0.3}MoO_3$ is a Mott insulator (i.e., an insulator or a semiconductor despite the fact that it has a partially filled band in a one-electron-band picture[30]), but recent experimental results[2a] are consistent with the conclusion[4] that red bronze is a regular semiconductor.

Step-Layers of Purple Bronzes and Magnéli Phases

Purple bronzes $A_{0.9}Mo_6O_{17}$ (A = Li, Na, K, Tl)[16,19] and Magnéli phases γ- and η-Mo_4O_{11}[8] are constructed from both MoO_6 octahedra and MoO_4 tetrahedra. Their Mo–O step-layers made up of MoO_6 octahedra can be described by employing projection views slightly different from those used for red and blue bronzes. We adopt a convention in which side- and top-projection views of an Mo_2O_{10} "ribbon" **14** are given by **15a** and **15b**, respectively. Then **16a** and **16b** are side- and

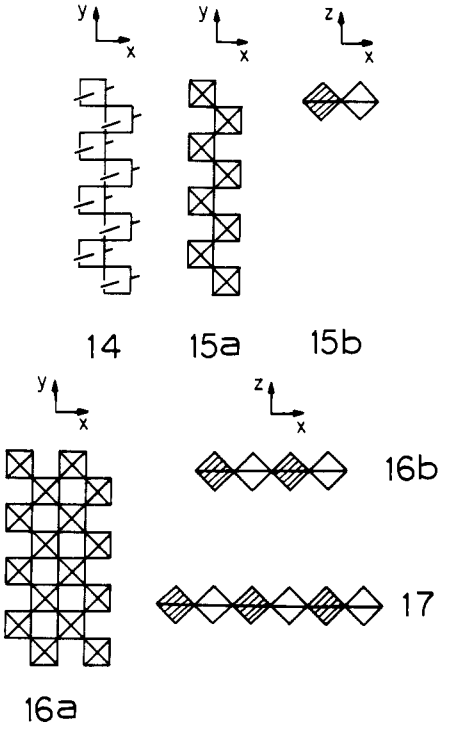

top-projection views of an Mo_4O_{18} ribbon, respectively, and **17** is a top-projection view of an Mo_6O_{28} ribbon. The Mo–O step-layers of MoO_6 octahedra found for purple bronze and the Magnéli phase are obtained by stacking ribbons (e.g., **16** and **17**) upon sharing their axial oxygen atoms. There are two ribbon-stacking modes, which are illustrated in **18** and **19** by employing Mo_2O_{10} ribbons. Between adjacent ribbons, all axial

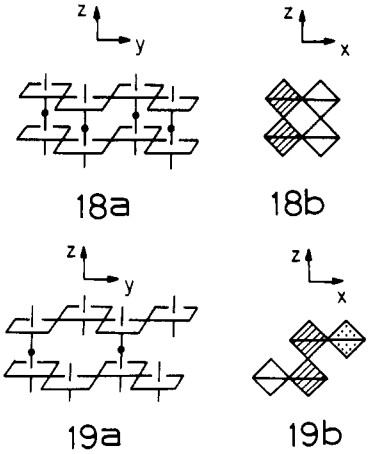

oxygen atoms are shared in **18a**, but only every other oxygen atom is shared in **19a**. Top-projection views of **18a** and **19a** are given by **18b** and **19b**, respectively. Then the Mo–O step-layers found for lithium purple bronze $Li_{0.9}Mo_6O_{17}$ and other purple bronzes $A_{0.9}Mo_6O_{17}$ (A = Na, K, Tl) are represented by **20** (Mo_8O_{30} step-layer) and **21** (Mo_4O_{15} step-layer), respectively, which are obtained by stacking Mo_4O_{18} ribbons **16** with the modes **18** and **19**, respectively. The Mo_6O_{22} step-layer **22** found for the Magneéli phase is constructed from Mo_6O_{18} ribbons **17** with the stacking mode **18**.

(27) (a) Mumme, W. G.; Watts, J. W. *J. Solid State Chem.* **1970**, *2*, 16. (b) *Structure Reports*; Pearson, W. B., Ed.; Oosthoek, Scheltema, Holkema: Utrecht, The Netherlands, 1957; Vol. 35A, p 227.
(28) Canadell, E.; Whangbo, M.-H. *Inorg. Chem.* **1989**, *28*, 1609.
(29) Travaglini, G.; Wachter, P. *Solid State Commun.* **1983**, *47*, 217.
(30) (a) Mott, N. F. *Metal-Insulator Transition*; Barnes and Noble: New York, 1977. (b) Brandow, B. H. *Adv. Phys.* **1977**, *26*, 651. (c) Whangbo, M.-H. *Acc. Chem. Res.* **1983**, *16*, 95. (d) Whangbo, M.-H. *J. Chem. Phys.* **1979**, *70*, 4963.

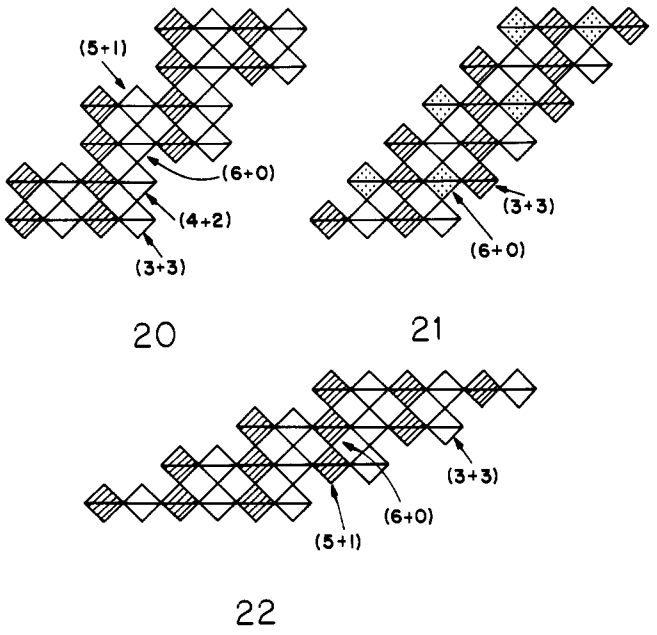

In purple bronze and the Magnéli phase, MoO_6 octahedra have all their oxygen atoms shared with neighboring MoO_6 octahedra, and also with MoO_4 tetrahedra when the number of adjacent MoO_6 octahedra is smaller than six. The MoO_6 octahedra of the layers **20**–**22** share six to three of their oxygen atoms with neighboring MoO_6 octahedra and, thus, share zero to three of their oxygen atoms with MoO_4 tetrahedra, which cap the faces of the Mo–O layers **20**–**22**. Consequently, each MoO_6 octahedron can be classified as an $(m + n)$ octahedron where m and n are the oxygen atom numbers shared with MoO_6 octahedra and MoO_4 tetrahedra, respectively. Then, there are four classes of MoO_6 octahedra to consider, i.e., $(m + n) = (6 + 0)$, $(5 + 1)$, $(4 + 2)$, or $(3 + 3)$.

In the Magnéli phases γ- and η-Mo_4O_{11}, every MoO_4 tetrahedron shares its oxygen atoms with two adjacent Mo_6O_{22} step-layers. Thus γ- and η-Mo_4O_{11} have three-dimensional (3D) crystal structures, and they differ only in the ways the oxygen atoms of MoO_4 tetrahedra are shared.[8] In $Li_{0.9}Mo_6O_{17}$,[19] one out of every two MoO_4 tetrahedra shares its oxygen atoms with two adjacent Mo_8O_{30} step-layers, thereby forming a 3D crystal structure as well. In other purple bronzes $A_{0.9}Mo_6O_{17}$ (A = Na, K, Tl),[16] no MoO_4 tetrahedron shares its oxygen atoms with two different Mo_4O_{15} step-layers, so that they have 2D crystal structures. In the purple bronzes $A_{0.9}Mo_6O_{17}$ (A = Li, Na, K, Tl) and the Magnéli phases γ- and η-Mo_4O_{11}, all MoO_6 octahedra have a type **2** distortion. The MoO_4 tetrahedra have in average much shorter Mo–O bonds than do the MoO_6 octahedra, and the short Mo–O bonds of the (3 + 3) and (4 + 2) octahedra are shorther than those of the (5 + 1) and (6 + 0) octahedra. Therefore, the lowest lying d-block bands of $Li_{0.9}Mo_6O_{17}$,[21] $K_{0.9}Mo_6O_{17}$,[18] and Mo_4O_{11}[10] are largely represented by the t_{2g}-block levels of the (5 + 1) and (6 + 0) octahedra of the Mo–O layers **20**, **21**, and **22**, respectively. Upon removal of the (3 + 3) and (4 + 2) octahedra, the layer **20** of $Li_{0.9}Mo_6O_{17}$ becomes isolated Mo_4O_{18} chains **18**,[21] but the layer **21** of $K_{0.9}Mo_6O_{17}$ and the layer **22** of Mo_4O_{11} still retain a layered structure.[10,18] Therefore, the lowest lying d-block bands of $Li_{0.9}Mo_6O_{17}$ are expected to exhibit 1D character in contrast to those of $K_{0.9}Mo_6O_{17}$ and Mo_4O_{11}. This is clearly seen from Figure 2, which shows dispersion relations of the lowest lying d-block bands calculated for $Li_{0.9}Mo_6O_{17}$,[21] $K_{0.9}Mo_6O_{17}$,[18] and Mo_4O_{11}.[10] Each of those three systems has partially filled bands and is expected to be a metal. In fact, all three systems are observed to be metals at room temperature.

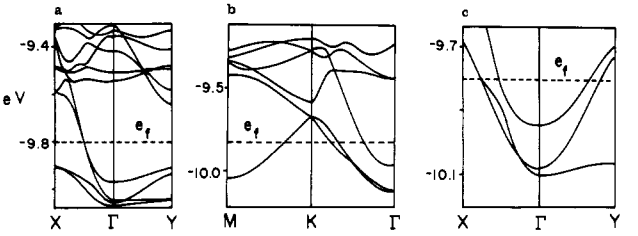

Figure 2. Dispersion relations calculated for the bottom portion of the t_{2g}-block bands in (a) $Li_{0.9}Mo_6O_{17}$, (b) $K_{0.9}Mo_6O_{17}$, and (c) Mo_4O_{11}. For a and c, the $\Gamma \rightarrow X$ and $\Gamma \rightarrow Y$ directions correspond to the chain and interchain directions, respectively. The Mo–O step-layer of $K_{0.9}Mo_6O_{17}$ is hexagonal, $M = (a^*/2, 0)$, and $K = (a^*/3, c^*/3)$.

Bridge p-Orbital Counting and Band Dispersion

As pointed out earlier, the band dispersions of Figures 1 and 2 can be explained by counting how many Mo–O–Mo bridges have nonvanishing p-orbital contributions at special points such as Γ, X, and Y.[4,10,18,21] The MoO_6 octahedra of the purple bronze and the Magnéli phase have a type **2** distortion, so that all three t_{2g} levels of each MoO_6 octahedron should be examined in constructing their lowest lying t_{2g}-block bands. Consequently, we need to consider both the axial bridging **23** and the equatorial bridging **24**. With respect to the

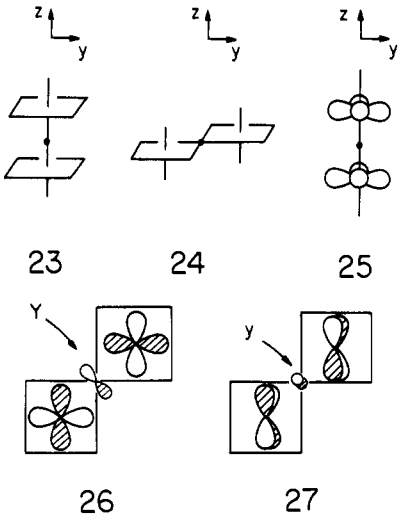

axial Mo–O–Mo bridge, the $x^2 - y^2$ orbital is a δ orbital (see **25**), and the xz and yz orbitals are π orbitals. No bridging-oxygen p orbital can mix between the neighboring δ orbitals at any wave vector point, while the bridging-oxygen π orbital can be present or absent between the adjacent π orbitals depending upon the wave vector. With respect to the equatorial Mo–O–Mo bridge, all t_{2g} levels of an MoO_6 octahedron are π orbitals so that the bridging-oxygen p orbital can be present or absent between the adjacent π orbitals depending upon the wave vector. When present, there occur two slightly different antibonding situations as illustrated in **26** and **27**. The bridging-oxygen p orbital

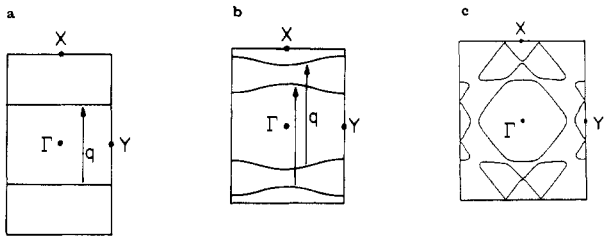

Figure 3. Fermi surfaces associated with the partially filled t_{2g}-block bands of (a) $Li_{0.9}Mo_6O_{17}$, (b) $K_{0.3}MoO_3$, and (c) Mo_4O_{11}. The Fermi surface nesting in a and b is indicated by the vector **q**.

makes stronger antibonding between the adjacent $x^2 - y^2$ orbitals (**26**) than between the adjacent xz or (yz) orbitals (**27**). The presence of such strong and weak antibonding interactions in Mo–O–Mo bridges may be distinguished by the symbols Y and y, respectivley, and the absence of antibonding interaction in a Mo–O–Mo bridge by the symbol N. In general, one Y interaction is as strong as twice the y interaction. Thus, by counting the Y, y, and N type interactions in various Mo–O–Mo bridges,[4,10,18,21] it is possible to explain why certain bands go up or down in energy as a function of wave vector.

Fermi Surface Nesting and Electronic Instability

For a layer band, the wave vectors (k_1, k_2) of the FBZ describe all allowed energy levels the band has. Thus, when a band is partially filled, some wave vectors of the FBZ are occupied (i.e., they lead to occupied band levels), and the remaining wave vectors of the FBZ are unoccupied (i.e., they lead to unoccupied band levels). Since wave vectors are equally probable, the area of the occupied wave vectors is proportional to the band filling so that half the FBZ is occupied for a half-filled band. The Fermi surface is defined as the boundary between the occupied and the unoccupied regions of the FBZ and occurs in the form of lines for layer bands.[10,15,18,21,24] The Fermi surfaces associated with the partially filled bands of $Li_{0.9}Mo_6O_{17}$,[21] $K_{0.3}MoO_3$,[15] and Mo_4O_{11}[10] are shown in parts a, b, and c, respectively, of Figure 3. When a piece of a Fermi surface can be translated by a vector **q** and superposed onto another piece of the Fermi surface, it is said that the two pieces are nested by **q**. For example, the Fermi surface of $Li_{0.9}Mo_6O_{17}$ (Figure 3a) consists of two flat lines (each doubly degenerate) nested by the vector $\mathbf{q} \cong 0.43(2\pi/b)$.[21] The Fermi surface of $K_{0.3}MoO_3$ (Figure 3b) consists of four curved lines, which are grouped into two pairs, each nested by the vector $\mathbf{q} \cong 0.75(2\pi/b)$.[15] The Fermi surface of Mo_4O_{11} (Figure 3c) has a complex pattern.[10] This pattern can be repeated by translation in wave vector space, and continuous Fermi surface lines can be selected in the resulting extended zone, as shown in Figure 4a.[10] It is clear from Figure 4a that a large part of the Fermi surface of Mo_4O_{11} is nested by the vector $\mathbf{q} \cong 0.23(2\pi/b)$.[10]

The electronic instability of a low-dimensional metal leading to a metal–insulator transition arises typically when its Fermi surface is nested.[31] Such an instability originates from orbital mixing between the filled and empty levels in the vicinity of the Fermi level.[31,32]

(31) Whangbo, M.-H. *Inorganic Compounds with Unusual Properties*; King, R. B., Ed.; American Chemical Society. In press.

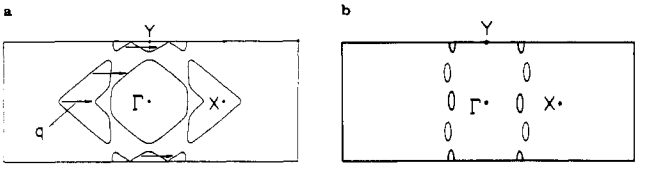

Figure 4. (a) Extended zone representation of the Fermi surface of Mo_4O_{11} (i.e., Figure 3c), where **q** represents the nesting vector. (b) Fermi surface expected to result from Figure 4a after being destroyed by the CDW associated with **q**.

Upon mixing of occupied and unoccupied levels, $\phi(\mathbf{k})$ and $\phi(\mathbf{k}')$, respectively, new orbitals $\psi(\mathbf{k}) \propto \phi(\mathbf{k}) + \lambda\phi(\mathbf{k}')$ and $\psi(\mathbf{k}') \propto -\lambda\phi(\mathbf{k}) + \phi(\mathbf{k}')$ may be obtained. These new orbitals introduce electron density waves given by the vector $\mathbf{q} = \mathbf{k} - \mathbf{k}'$ [e.g., for a 1D system with repeat distance d, these orbitals will introduce an electron-density modulation with the periodicity given by $(2\pi/d)/q$].[31] The density waves resulting from the orbitals are out of phase in that $\phi(\mathbf{k})$ accumulates electron density where $\phi(\mathbf{k}')$ depletes electron density. When a Fermi surface has a nesting vector **q**, this orbital mixing can be carried out throughout the wave vectors of the FBZ, thereby leading to sets of new orbitals $\psi(\mathbf{k})$ and $\psi(\mathbf{k}')$ differing in their wave vectors by **q**. Thus a CDW state is obtained when only one set of orbitals $\psi(\mathbf{k})$ are occupied, while an SDW state is derived when the set of orbitals $\psi(\mathbf{k})$ and $\psi(\mathbf{k}')$ are filled with up-spin and down-spin electrons, respectively.[31,32] Both CDW and SDW states are insulating in nature because a band gap is introduced by the orbital mixing. In other words, orbital mixing induced by nesting removes the Fermi surface. The driving force leading to a CDW or an SDW state is the energy gain that results from the interactions of occupied levels $\phi(\mathbf{k})$ with unoccupied levels $\phi(\mathbf{k}')$, i.e., $\langle\phi(\mathbf{k})|H'|\phi(\mathbf{k}')\rangle$, where the perturbation H' causing the orbital mixing is lattice vibration and electron–electron repulsion for CDW and SDW states, respectively.

The additional periodicity of electron-density distribution introduced by a CDW is observed as diffuse peaks or superlattice spots in X-ray and electron-diffraction measurements.[31,33] Thus the electronic instability associated with the nesting vector $\sim 0.23(2\pi/b)$ in γ- and η-Mo_4O_{11}[9b] and that with the nesting vector $\sim 0.75(2\pi/b)$ in $K_{0.3}MoO_3$[14] are all found to be CDWs. The observed CDW **q** vector of $K_{0.3}MoO_3$ depends upon temperature, i.e., **q** is $\sim 0.72(2\pi/b)$ at room temperature and increases gradually to $\sim 0.75(2\pi/b)$ upon lowering of the temperature.[14] This phenomenon is caused by the presence of an empty band lying very close to the Fermi level (see Figure 1b).[14d,15] Thermal excitation of electrons into this band leaves fewer than three electrons for the bottom two bands, thereby decreasing the q value. In Figure 4a, the nesting **q** is incomplete since the Fermi surface has some pieces not nested by **q** (i.e., those approximately parallel to $\Gamma \rightarrow Y$). In such a case, CDW formation associated with **q** does not remove these pieces, but leads to elongated ellipse-like pockets comprising them as schematically shown in Figure 4b. Nesting among such Fermi surface pockets would be

(32) (a) Whangbo, M.-H. *J. Chem. Phys.* **1980**, *73*, 3854. (b) Whangbo, M.-H. *J. Chem. Phys.* **1981**, *75*, 4983.

(33) Pouget, J. P. In *Low Dimensional Electronic Properties of Molybdenum Bronzes and Oxides*; Schlenker, C., Ed.; Reidel: Dordrecht, The Netherlands, 1989; Chapter 3.

responsible for another resistivity anomaly found for η-Mo_4O_{11} at 30 K.[9]

No unambiguous evidence for CDW or SDW has been found in $Li_{0.9}Mo_6O_{17}$, so it is not clear whether its resistivity upturn occurring at ~25 K is caused by a CDW or an SDW state associated with the Fermi surface nesting. Upon further lowering of the temperature, $Li_{0.9}Mo_6O_{17}$ is found to become a superconductor at 1.9 K.[20] As in the case of CDW and SDW states, a superconducting state also involves orbital mixing (in an indirect manner) between filled and unfilled band levels.[31] Charge carriers of a superconducting state are pairs of electrons having opposite wave vectors, which are described by product functions $\phi(\mathbf{k})\phi(-\mathbf{k})$.[31,34] The driving force leading to superconductivity comes from the interactions (i.e., mixings) of occupied pair functions $\phi(\mathbf{k})\phi(-\mathbf{k})$ with unoccupied pair functions $\phi(\mathbf{k}')\phi(-\mathbf{k}')$, i.e., $\langle\phi(\mathbf{k})\phi(-\mathbf{k})|H'|\phi(\mathbf{k}')\phi(-\mathbf{k}')\rangle$, where the perturbation H' responsible for this mixing is electron–phonon interaction.[34] Depending upon the nature and strength of the perturbations causing orbital mixing, a normal metal with a nested Fermi surface may in principle reach a CDW, an SDW, or a superconducting state upon lowering of the temperature. In most cases, Fermi surface nesting leads to a metal–insulator transition such as CDW or SDW formation. Occurrence of a superconducting state despite the presence of a Fermi surface nesting would mean that the interaction matrix elements $\langle\phi(\mathbf{k})|H'|\phi(\mathbf{k}')\rangle$ responsible for CDW or SDW formation are very small. In cases in which the relative stabilities of CDW, SDW, and superconducting states are similar, preference of one state over the other would be delicately balanced by a change in temperature and pressure. This appears to be the case for $Li_{0.9}Mo_6O_{17}$. Experimental confirmation of CDW or SDW in $Li_{0.9}Mo_6O_{17}$ would be of interest.

(34) (a) Bardeen, J.; Cooper, L. N.; Schrieffer, J. R. *Phys. Rev.* **1957**, *108*, 1175. (b) Grassie, A. D. C. *The Superconducting State*; Sussex University Press: London, 1975; Chapter 2. (c) Solymar, L.; Walsh, D. *Lectures on the Electrical Properties of Materials*, 4th ed.; Oxford University Press: Oxford, England, 1988; Chapter 14.

Concluding Remarks

All molybdenum oxide metals contain Mo–O steplayers made up of distorted MoO_6 octahedra, and their unit cells, being large in size and complex in pattern, contain several nonequivalent Mo atoms. Due to the very low d-electron count on Mo in every molybdenum oxide metal, only certain kinds of MoO_6 octahedra contribute their lowest lying t_{2g} levels to form the highest occupied bands responsible for its metallic properties. One can readily recognize such MoO_6 octahedra as the ones whose short Mo–O bonds are long compared with those of other MoO_6 octahedra, because the t_{2g}-block levels are antibonding between Mo and O. Dispersion characteristics of the highest occupied bands are explained by counting in how many Mo–O–Mo bridges the oxygen p orbital can mix between adjacent t_{2g} orbitals at a few special wave vector points. Metals with nested Fermi surfaces, such as the molybdenum oxide metals, are susceptible to a metal–insulator transition leading to a CDW or an SDW state. When CDW and SDW instabilities are weak, a metal may even reach a superconducting state, as in the case of $Li_{0.9}Mo_6O_{17}$. CDW, SDW, and superconducting states are all described in terms of orbital mixing between the occupied and unoccupied levels of a normal metallic state near the Fermi level. What structural factors govern the relative stabilities of CDW, SDW, and superconducting states at low temperatures is an important problem to study.

This work was supported by NATO, Scientific Affairs Division, and also by DOE, Office of Basic Sciences, Division of Materials Sciences, under Grant DE-FG05-86ER45259.

A New Two-Parameter Mass Spectrometry

JOHN H. D. ELAND

Physical Chemistry Laboratory, South Parks Road, Oxford, U.K.

Received May 1, 1989 (Revised Manuscript Received August 9, 1989)

I. Introduction

This Account describes a form of mass spectrometry whose spectra are three-dimensional, showing intensity as a function of two mass parameters. The technique, which is based on charge separation of doubly charged ions, is particularly suitable for the study of fragmentation mechanisms and may eventually find applications in structure determination and analysis.

In regular mass spectrometry, ions created by one of several ionization methods are separated according to their mass-to-charge ratios (m/z) and a spectrum of intensity as a function of m/z is recorded. In the present technique,[1,2] by contrast, the primary process of interest is dissociative double ionization,

$$p + h\nu \rightarrow [p^{2+}] \rightarrow m_1^+ + m_2^+ (+m_3)$$

and intensity is recorded as a function of the two m/z values of the ionic products. A photon is shown as the

John H. D. Eland was born in Shropshire, England, on August 6, 1941. He read Chemistry at Oxford under E. J. Bowen and obtained the D.Phil. degree under C. J. Danby. He has since worked in Freiburg with B. Brehm, in Paris with S. Leach, at Argonne with J. Berkowitz, and most recently at Okazaki with K. Kimura. His other research activities include photoelectron spectroscopy and various combinations of electron and ion spectrometries using coincidence techniques, all more or less related to the formation and reactions of molecular ions. His home base is at Oxford, where he is a University Lecturer in Physical Chemistry and a Fellow of Worcester College.

(1) Eland, J. H. D.; Wort, F. S.; Royds, R. N. *J. Electron Spectrosc. Relat. Phenom.* **1986**, *41*, 297-309.
(2) Frazinski, L. J.; Stankiewicz, M.; Randall, K. J.; Hatherley, P. A.; Codling, K. *J. Phys. B* **1986**, *19*, L819-824.

0001-4842/89/0122-0381$01.50/0